Transport in Porous Media (2020) 132:405–421
https://doi.org/10.1007/s11242-020-01398-w

On the Interfacial Flow Over Porous Media Composed of Packed Spheres: Part 2-Optimal Stokes–Brinkman Coupling with Effective Navier-Slip Approach

Jin Gang Lu[1] · **Wook Ryol Hwang**[1]

Received: 26 September 2019 / Accepted: 25 February 2020 / Published online: 4 March 2020

Abstract
The Stokes–Brinkman coupling has been employed to investigate the flow through porous media composed of packed spheres. By matching the slip velocity using the Navier-slip condition, optimal values of the effective viscosity in the continuous stress condition and of the stress jump coefficient in the stress jump condition could be accurately determined. The correlations between the slip length (which has been accurately determined in Part 1) and the effective viscosity as well as the stress jump coefficient have been specified. The accuracy of these two optimal parameters (i.e., the effective viscosity and stress jump coefficient) has been assessed by comparing the velocity profiles in both the fluid and porous regions obtained from the Stokes–Brinkman coupling, with those obtained from the corresponding direct simulations. It is observed that the stress jump condition with the optimal stress jump coefficient yields a superior prediction in the velocity field. The optimal effective viscosity decreases as the solid volume fraction increases, whereas the stress jump coefficient increases with the solid volume fraction. By selecting the optimal parameters, the Stokes–Brinkman coupling with both the continuous stress condition and stress jump condition is applied to solve two example flow problems: a stick–slip–stick flow and a pressure-driven flow in a rectangular channel. Both the stress conditions in the Stokes–Brinkman coupling exhibit good performances in reproducing the velocity fields within the entire domain.

Keywords Stokes–Brinkman coupling · Effective viscosity · Stress jump coefficient · Navier-slip · Packed spheres

1 Introduction

Porous media composed of packed spheres are widely used in a variety of industrial processes, e.g., chemical reactors (Takhirov 2013; Lu et al. 2018), heat transfer and storage (Varahasamy and Fand 1996; Esence et al. 2019), sound absorption (Gasser et al. 2005),

✉ Wook Ryol Hwang
wrhwang@gnu.ac.kr

[1] School of Mechanical and Aerospace Engineering, Research Center for Aircraft Parts Technology (ReCAPT), Gyeongsang National University, Jinju 52828, Korea

filtration (Chellam and Wiesner 1993), and composites manufacturing (Llorca et al. 1997; Segurado and Llorca 2002). It is established that when a fluid flows over porous media, the velocity within a narrow boundary layer adjacent to the fluid/pore interface decreases rapidly from the slip velocity to the Darcy velocity. Only a few experiments concerning the local flow field measurement near the interface are reported in the literature, for example, Vignesadler et al. (1987) and Saleh et al. (1993). In theoretical works, Brinkman (1949) added a term containing a second-order derivative of the velocity in conjunction with a pseudo viscosity (effective viscosity) into Darcy's law to account for the substantial viscous dissipation within the boundary layer. Therefore, the Brinkman equation is physically and mathematically preferable than the Darcy's law for describing the flow through porous media. In case of slow flows over small-scale porous architectures, which are often encountered in packed spheres, the combination of the Stokes equation in a fluid region and the Brinkman equation in a porous region, the so-called Stokes–Brinkman coupling, has been widely employed in analyses and numerical simulations of dual-scale flow through and over porous media (Neale and Nader 1974; Breugem 2007; Hwang et al. 2011). In this work, by introducing a parameter λ (0 in the fluid region and 1 in the porous media), the Stokes–Brinkman coupling can be expressed by a single equation as follows:

$$-\nabla p + \mu \nabla^2 \boldsymbol{u} + \lambda \left(\left(\mu_{\mathrm{e}} - \mu \right) \nabla^2 \boldsymbol{u} - \frac{\mu}{K} \boldsymbol{u} \right) = 0. \tag{1}$$

The symbols p, μ, μ_{e}, K, and $\mathbf{u}$ are the pressure, fluid viscosity, effective viscosity, permeability, and velocity vector, respectively. A critical issue in Stokes–Brinkman coupling is the determination of the interfacial boundary condition. Across the interface over the porous media, the velocity continuity must be satisfied and, as for the force balance, either one of two types of stress boundary conditions can be employed: One is the continuous stress condition and the other is stress jump condition. According to the work pioneered by Ochoa-Tapia and Whitaker (1995a, b), a stress jump condition at the interface between the fluid and porous media is developed based on the non-local volume-averaging technique such that

$$\boldsymbol{n} \cdot \left(\boldsymbol{\sigma}_{\mathrm{p}} - \boldsymbol{\sigma}_{\mathrm{f}} \right) = \frac{\mu}{\sqrt{K}} \boldsymbol{T} \cdot \boldsymbol{u}, \qquad \boldsymbol{T} = \beta \boldsymbol{I}. \tag{2}$$

The subscripts 'f' and 'p' denote the fluid and porous media, respectively. The symbols $\boldsymbol{n}, \boldsymbol{\sigma}, \boldsymbol{T}, \boldsymbol{I}$ and, β are the outward normal vector at the interface, stress tensor, stress jump tensor, identity tensor and, stress jump coefficient, respectively. The continuous stress condition is defined by vanishing stress jump coefficient $\beta = 0$ along with the additional effective viscosity μ_{e}. The flow characteristics at the interface are controlled by the stress jump coefficient and the effective viscosity, depending on the model, and they are functions of the porous architecture, as it should be. In addition, there must be optimal values of the effective viscosity in the Brinkman equation for the continuous stress boundary condition and of the stress jump coefficient for the stress jump boundary condition, which best mimic the flow characteristics at the interface. Once determined, they need to facilitate an accurate reproduction of the velocity profiles in both the fluid region and porous media. In particular, the slip velocity, its slope at the interface, and the boundary layer thickness have to be predicted accurately.

In the literature, there is no agreement on determining the optimal value of the effective viscosity $\left(\mu_{\mathrm{e}}\right)$. In most cases, it is regarded as identical to the fluid viscosity, i.e., $\mu_{\mathrm{e}}/\mu = 1$, for simplification (Hwang and Advani 2010; Tamayol et al. 2012, 2013). In

the original work by Brinkman (1949), it was identified as the effective viscosity of particle suspension such that $\mu_e/\mu = 1 + 2.5\phi_s$, by considering the flow in porous media as analogous to the swarm of particles in a dilute regime with the solid fraction ϕ_s. Martys et al. (1994) applied the finite difference method to simulate flows over randomly packed spheres. By matching the slip velocity from the direct simulation with that from the theoretical solution of the Stokes–Brinkman coupling, μ_e is obtained and it was observed to be higher than the fluid viscosity. Starov and Zhdanov (2001) derived the expression of μ_e as $\mu_e/\mu = 1/\left(1-\phi_s\right)^{5/2}$, for the flow in porous media composed of equally sized spherical particles. It implies that μ_e is always larger than the fluid viscosity. Valdes-Parada et al. (2007) obtained the implicit expression of μ_e by up-scaling the Stokes equation using the volume averaging method and reported that μ_e decreases with the porosity.

As indicated by Ochoa-Tapia and Whitaker (1995a, b), in the stress jump boundary condition, the value of μ_e is fixed as $\mu_e/\mu = 1/\left(1-\phi_s\right)$. This leaves another key parameter, the stress jump coefficient (β), to be determined. As illustrated in Eq. (2), the stress jump coefficient tensor $\boldsymbol{T}$ can be simplified as an isotropic tensor $\beta\boldsymbol{I}$ and is based on the assumption that the stress discontinuity is present only in the flow direction. The optimal choice of the stress jump coefficient is also an argumentative issue. Ochoa-Tapia and Whitaker (1995b) reported that a stress jump coefficient ranging from -1 to 1.47 provides good agreements for the fractional increase in the flow rate with the corresponding experimental results from Beavers and Joseph (1967). Angot (2011) pointed out that the well-posedness of the Stokes–Brinkman problem requires the stress jump coefficient being nonnegative. Goyeau et al. (2003) introduced a heterogeneous continuously varying transition layer between homogenized fluid and porous regions and derived the stress jump coefficient as an explicit function of the velocity variations and effective properties of the transition layer. Min and Kim (2005) presented a novel method to analyze the fluid flow in a pore/fluid composite system. By comparing the interfacial conditions with the stress jump condition proposed by Ochoa-Tapia and Whitaker (1995b), the stress jump coefficient has been determined in terms of the porosity, Darcy number, and pore diameter. Chandesris and Jamet (2007) presented a linear dependence of the stress jump coefficient on the location of the fluid/pore interface by imposing the constraint of conservation of the redefined friction surface-excess force. Valdes-Parada et al. (2009) combined the generalized transport equations with the two-domain approach developed by Goyeau et al. (2003) and derived the expression of the stress jump coefficient as a function of the porosity, the Darcy number, the width of the inter-region, and the spatial variations of porosity and permeability.

In this work, the Stokes–Brinkman coupling with either the continuous stress condition or the stress jump condition at the fluid/pore interface is employed to describe a channel flow over porous media composed of packed spheres. First, we derive the optimal expressions of μ_e in the continuous stress condition and β in the stress jump condition, by matching the slip velocity using the Navier-slip condition. The correlations between the slip length and μ_e as well as β are determined. Then, the accuracy of the optimal values of these two parameters (i.e., μ_e and β) are assessed by comparing the velocity profiles from the direct simulation and those from the Stokes–Brinkman coupling with both the continuous and jump stress conditions. Finally, with these two optimal parameters, the Stokes–Brinkman coupling is employed to investigate two example flow problems: a stick–slip–stick flow and a rectangular channel flow. The performances of both the continuous stress condition and stress jump condition will be investigated.

2 Optimal Effective Viscosity and Stress Jump Coefficient

2.1 Derivation of Optimal Effective Viscosity and Stress Jump Coefficient

In this section, we present the analytic solution of the Stokes–Brinkman coupling with the optimal effective viscosity in the continuous stress condition and with the stress jump coefficient in the stress jump condition. By matching the slip velocity at the fluid/pore interface from both the cases (continuous/jump stress condition) with that from the Navier-slip condition, the correlations between the slip length and μ_e as well as β can be obtained.

Before deriving the optimal expressions of μ_e and β, we briefly review the Navier-slip boundary condition. (See Part 1 for details.) Figure 1a shows a pressure-driven flow over porous media composed of packed spheres, with the coordinate system. The entire domain can be decomposed into two regions: the pure fluid region ($0 < z < H$) and porous region ($z < 0$). In Part 1, we reported that the actual porous architecture can be replaced by the effective Navier-slip condition over an imaginary smooth interface between the pure fluid and porous media. The slip velocity as well as the velocity profiles in the fluid channel can be reproduced accurately with this. The Navier-slip condition can be written as $\boldsymbol{u}_{\text{slip}} = \boldsymbol{b} \cdot (\boldsymbol{n} \cdot \nabla \boldsymbol{u})$. $\boldsymbol{b}$ and $\boldsymbol{u}_{\text{slip}}$ are the slip length tensor and slip velocity vector, respectively. In a simple pressure-driven channel flow over a flat surface, it becomes

$$u_{\text{slip}} = b\frac{\mathrm{d}u}{\mathrm{d}z}. \tag{3}$$

In Part 1, the effective slip length b has been obtained following the flow rate matching method by Beavers and Joseph (1967): $b = ((Q^* - 1)H - 6K/H)/(4 - Q^*)$, Q^* is the flow rate ratio (the ratio of the flow rate under the slip boundary condition to that under the no-slip boundary condition), and H is the channel height. We note that the slip length 'b' for packed spheres can be isotropic and the slip length tensor $\boldsymbol{b} = b\boldsymbol{I}$. Assuming that the top wall ($z = H$) is subjected to the no-slip boundary condition, and considering the original slip boundary condition by Beavers and Joseph's, i.e.,

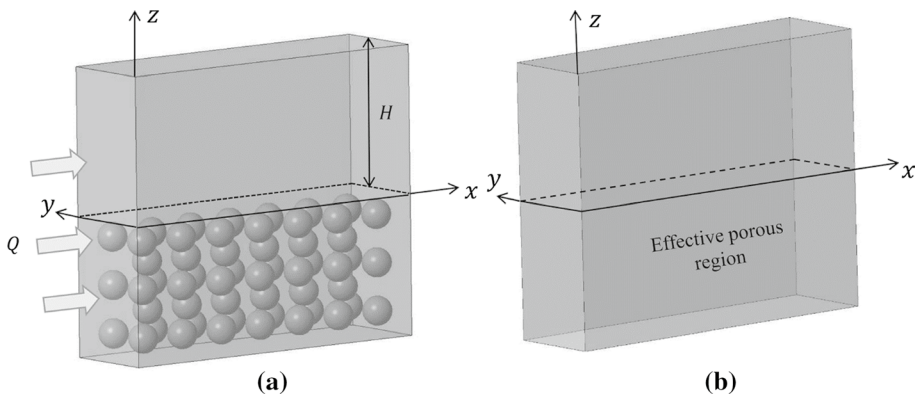

Fig. 1 Schematic description of unidirectional flow over (**a**) porous medium composed of packed spheres and over (**b**) fictitious porous region characterized by permeability and effective viscosity

$\mathrm{d}u/\mathrm{d}z = \alpha_{\mathrm{BJ}}/\sqrt{K}\left(u - u_{\mathrm{D}}\right)$ (u_{D} is the Darcy velocity, and α_{BJ} is the dimensionless slip coefficient [$\alpha_{\mathrm{BJ}} = \sqrt{K}/b$, see Lu et al. (2017)], the velocity profile in the fluid channel can be expressed as

$$u(z) = \left(\frac{H/\sqrt{K}\left(H/\sqrt{K} + 2\sqrt{K}/b\right)}{2\left(1 + \sqrt{K}/b \cdot H/\sqrt{K}\right)} + \frac{\sqrt{K}/b\left(H^2/K - 2\right)}{2\left(1 + \sqrt{K}/b \cdot H/\sqrt{K}\right)} \left(\frac{z}{\sqrt{K}} \right) - \frac{1}{2}\left(\frac{z}{\sqrt{K}} \right)^2 \right) \cdot u_{\mathrm{D}}. \tag{4}$$

The slip velocity at the interface ($z = 0$) is then

$$u_{\mathrm{s}} = \frac{H/\sqrt{K} \cdot \left(H/\sqrt{K} + 2\sqrt{K}/b\right)}{2\left(1 + \sqrt{K}/b \cdot H/\sqrt{K}\right)} \cdot u_{\mathrm{D}}. \tag{5}$$

In Part 1, we proposed a master fitted curve by introducing a parameter called the dimensionless free surface area A^* (the ratio between the free slip area and the surface area of a unit cube) to compute the slip length:

$$b^* = A^{*4} + 0.23, \qquad b^* = b/R, \tag{6}$$

where R is the radius of the packed sphere. The correlation between A^* and the solid volume fraction ϕ_{s} is expressed as $A^* = 1 - N\pi^{1/3}\phi_{\mathrm{s}}^{2/3}/(4n/3)^{2/3}$. N denotes the number of spheres within the top surface of a unit cubic structure (see Fig. 3 in Part 1). For the single cubic (SC) and body centered cubic (BCC) packing structures, N is 1; for the face centered cubic (FCC) structure, $N = 2$. n is the number of spheres within a unit cubic structure, and it is equal to one, two, and four for the SC, BCC and FCC structures, respectively.

As reported in Part 1, an imaginary smooth interface with the effective Navier-slip boundary condition can accurately reproduce the slip velocity as well as the velocity profile in the pure fluid channel. However, to account for the flow in porous media, an effective porous region (Fig. 1b) characterized by K and μ_{e} is introduced to replace the actual porous architecture (Fig. 1a). The flow in the fluid region can be described by the Stokes equation, whereas that in the effective porous region can be described by the Brinkman equation. The combination of the Stokes and Brinkman equation, the so-called Stokes–Brinkman coupling, is then applied to describe the flow in the entire region [see Eq. (1)]. At the fluid/pore interface, the velocity is continuous, i.e., $u_{\mathrm{f}} = u_{\mathrm{p}}$. Meanwhile, either the continuous or jump stress condition can be applied, as illustrated in Eq. (2), with β being zero for the continuous stress condition. Note that, the effective viscosity in the stress jump condition is indicated to be $\mu_{\mathrm{e}}/\mu = 1/\left(1 - \phi_{\mathrm{s}}\right)$ by Ochoa-Tapia and Whitaker (1995a, b) in their model. Within the porous media away from the interface, the effect of the viscous stress gradually vanishes. This implies that the Darcy's law, i.e., $u_{\mathrm{p}} = -K/\mu \mathrm{d}p/\mathrm{d}x$ is recovered: $u_{\mathrm{p}} \to u_{\mathrm{D}}$, $z \to -\infty$. The remaining boundary (top surface) is considered as a no-slip wall. Based on the governing equation [Eq. (1)] and the boundary conditions above, the velocity profiles in the entire domain for the Stokes–Brinkman coupling with both the continuous and jump stress conditions can be obtained. For the continuous stress condition, the velocity profiles in the channel and effective porous region can be expressed by Eqs. (7) and (8), respectively:

$$u_f = u_D\left(\frac{\left(H^2/K + 2H/\sqrt{K}\sqrt{\mu_e/\mu}\right)}{2\left(1+\sqrt{\mu_e/\mu}\cdot H/\sqrt{K}\right)} + \frac{\left(H^2/K-2\right)\sqrt{\mu_e/\mu}}{2\left(\sqrt{K}+\sqrt{\mu_e/\mu}\cdot H\right)}z - \frac{z^2}{2K}\right), \tag{7}$$

$$u_p = u_D\left(1 + \frac{H^2/K-2}{2\left(1+H/\sqrt{K}\sqrt{\mu_e/\mu}\right)}e^{\sqrt{\mu/\mu_e}\frac{z}{\sqrt{K}}}\right). \tag{8}$$

For the stress jump condition, the velocity profiles in the channel and porous region are

$$u_f = u_D\left(\frac{\left(H^2/K + 2H/\sqrt{K}\sqrt{1/(1-\phi_s)}\right)}{2\left(1-\beta H/\sqrt{K}+\sqrt{1/(1-\phi_s)}\cdot H/\sqrt{K}\right)} + \frac{\left(H^2/K-2\right)\sqrt{1/(1-\phi_s)}-\beta H^2/K}{2\left(\sqrt{K}-\beta H+\sqrt{1/(1-\phi_s)}\cdot H\right)}z - \frac{z^2}{2K}\right), \tag{9}$$

$$u_p = u_D\left(1 + \frac{H^2/K-2+2\beta H/\sqrt{K}}{2\left(1-\beta H/\sqrt{K}+H/\sqrt{K}\sqrt{1/(1-\phi_s)}\right)}e^{\sqrt{1-\phi_s}\frac{z}{\sqrt{K}}}\right). \tag{10}$$

The slip velocity at the interface can be obtained by setting z as zero in either Eq. (7) or Eq. (8) for the continuous stress condition and in either Eq. (9) or Eq. (10) for the stress jump condition. This can be written in terms of the effective viscosity and stress jump coefficient, respectively

$$u_s = \frac{\left(H^2/K + 2H/\sqrt{K}\sqrt{\mu_e/\mu}\right)}{2\left(1+\sqrt{\mu_e/\mu}\cdot H/\sqrt{K}\right)}\cdot u_D, \qquad \text{(Continuous stress)} \tag{11}$$

$$u_s = \frac{\left(H^2/K + 2H/\sqrt{K}\sqrt{1/(1-\phi_s)}\right)}{2\left(1-\beta H/\sqrt{K}+\sqrt{1/(1-\phi_s)}\cdot H/\sqrt{K}\right)}\cdot u_D. \qquad \text{(Stress jump)} \tag{12}$$

The closed form expressions of the effective viscosity and stress jump coefficient can then be obtained by equating the slip velocity obtained using the Navier-slip boundary condition with the slip length [Eq. (5)], to those subjected to either the continuous stress condition [Eq. (11)] or stress jump condition [Eq. (12)]. The expressions of the relative effective viscosity (normalized by the fluid viscosity) and the stress jump coefficient can be described as follows:

$$\frac{\mu_e}{\mu} = \frac{K}{b^2}, \tag{13}$$

$$\beta = \frac{\left(1/\left(1-\phi_s\right) - \sqrt{K}/b\right)\left(H^2/2K - 1\right)}{H^2/2K + H/b}. \tag{14}$$

Substituting the approximate expression of the slip length [Eq. (6)] into Eqs. (13) and (14), and considering the correlation between the dimensionless free surface area and solid volume fraction, the optimal relative effective viscosity and stress jump coefficient can be expressed in closed forms in terms of the permeability, porosity, and porous architecture:

$$\frac{\mu_e^{\mathrm{OPT}}}{\mu} = \left(1.064\left(1 - N\pi^{1/3}\phi_s^{2/3}/\left(4n/3\right)^{2/3}\right)^{3.929} + 0.23\right)^{-2} \cdot K', \tag{15}$$

$$\beta^{\mathrm{OPT}} = \frac{\left(1/\left(1-\phi_s\right) - \sqrt{K'}\left(1.064\left(1 - N\pi^{1/3}\phi_s^{2/3}/\left(4n/3\right)^{2/3}\right)^{3.929} + 0.23\right)^{-1}\right)\left((H/R)^2/2K' - 1\right)}{(H/R)^2/2K' + (H/R)/\left(1.064\left(1 - N\pi^{1/3}\phi_s^{2/3}/\left(4n/3\right)^{2/3}\right)^{3.929} + 0.23\right)}. \tag{16}$$

The superscript 'OPT' in Eqs. (15) and (16) indicates that the values of both the relative effective viscosity and stress jump coefficient provided here are optimal. The symbol K' denotes the normalized permeability (normalized by the square of the sphere radius). It can be obtained by the Carman–Kozeny model, i.e., $K' = A\left(1-\phi_s\right)^3/\phi_s^2$. In Part 1, we reported that for porous media composed of packed spheres, the Carman–Kozeny constant A can be decomposed into two factors, i.e., $A = a\phi_s^b$. The parameters a and b are specified as 0.0343 and 0.610 for the SC structure, 0.0320 and 0.590 for the FCC structure, 0.0323 and 0.598 for the BCC structure, respectively. It is noted from Eqs. (15) and (16) that unlike the optimal relative effective viscosity, the stress jump coefficient depends on the dimensionless channel height (H/R). In this study, the channel height is considered much larger than the square root of permeability, i.e., $H/\sqrt{K} \gg 1$. Now let us recall Eq. (14) and divide both the top and bottom by $H^2/2K$, Eq. (14) becomes

$$\beta \approx \frac{1/\left(1-\phi_s\right) - \sqrt{K}/b}{1 + \left(2K/R^2\right)\cdot(R/b)\cdot(R/H)} = \frac{1/\left(1-\phi_s\right) - \sqrt{K}/b}{1 + \left(2K'/b^*\right)\cdot(R/H)} \approx \frac{1}{1-\phi_s} - \frac{\sqrt{K}}{b}. \tag{17}$$

As indicated in Table 1 of Part 1, when the channel height is large enough (e.g., $H/R > 32$, which is common for flows through porous media), $\left(2K'/b^*\right)\cdot(R/H) \ll 1$. The stress jump coefficient is then approximated to be $1/\left(1-\phi_s\right) - \sqrt{K}/b$, which can be considered independent of the channel height in many practical situations. Therefore, both the relative effective viscosity and stress jump coefficient might be considered as a property of the porous medium itself.

Figure 2 shows the optimal values of the relative effective viscosity and stress jump coefficient as functions of the solid volume fraction for three packing structures. Figure 2a shows that, for various packing structures, the relative effective viscosity decreases as the solid volume fraction increases. For the same solid volume fraction, the SC structure has the highest relative effective viscosity, whereas the BCC structure has the lowest one. As the solid volume fraction increases, the value of the relative effective viscosity ranges from 2.329 to 0.255 for the SC packing structure, from 0.976 to 0.05 for

Table 1 Optimal relative effective viscosity, stress jump coefficient in conjunction with normalized permeability as a function of solid volume fraction for various porous architectures. The dimensionless channel height is $H/R = 32$.

ϕ_s	SC			BCC			FCC		
	K/R^2	μ_e^{OPT}/μ	β^{OPT}	K/R^2	μ_e^{OPT}/μ	β^{OPT}	K/R^2	μ_e^{OPT}/μ	β^{OPT}
0.1	0.613	2.329	−0.439	0.595	0.976	0.063	0.598	1.461	−0.145
0.2	0.165	1.275	−0.011	0.159	0.547	0.371	0.160	0.812	0.212
0.3	0.062	0.742	0.329	0.059	0.317	0.627	0.059	0.466	0.507
0.4	0.026	0.431	0.630	0.024	0.180	0.863	0.024	0.257	0.780
0.5	0.012	0.255	0.906	0.010	0.097	1.10	0.009	0.132	1.048
0.6	–	–	–	0.004	0.050	1.357	0.004	0.061	1.333
0.7	–	–	–	–	–	–	0.001	0.024	1.671

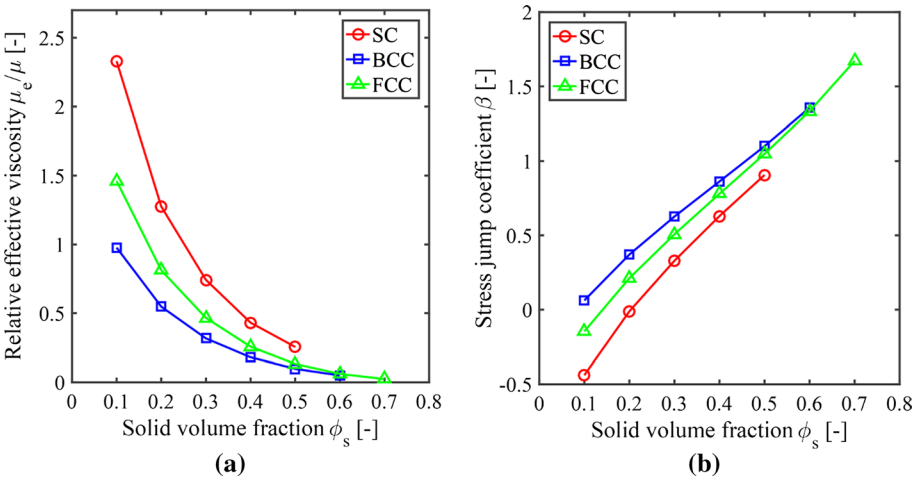

Fig. 2 Dependences of solid volume fraction on (**a**) relative effective viscosity and (**b**) stress jump coefficient for various packing structures of spheres. The dimensionless channel height is $H/R = 32$.

the BCC structure and from 1.461 to 0.024 for the FCC packing structures. As shown in Fig. 2b, in contrast to the effective viscosity, the stress jump coefficient increases with the solid volume fraction for various packing structures. For an equal solid volume fraction, the BCC structure has the highest stress jump coefficient, while the SC structure has the lowest one. Consistent with Ochoa-Tapia and Whitaker (1995a, b), the value of the stress jump coefficient is observed to be $O(1)$ and can be either positive or negative. Specifically, the ranges of the stress jump coefficient are from −0.439 to 0.906 for the SC structure, from 0.063 to 1.357 for the BCC structure and from −0.145 to 1.671 for the FCC structure, respectively. Detailed data for the optimal relative effective viscosity and stress jump coefficient in conjunction with the normalized permeability for the three packing structures are listed in Table 1.

2.2 Validation of Optimal Effective Viscosity and Stress Jump Coefficient

Having characterized the optimal expressions of the effective viscosity in the continuous stress condition and of the stress jump coefficient in the stress jump condition, the accuracy of these two parameters need to be validated. To do so, two flow simulations are implemented: a direct simulation of flow over the actual porous architecture (Fig. 3a) and the optimal Stokes–Brinkman coupling (Fig. 3b) with both the continuous and jump stress conditions. To reduce computational cost for the direct simulation, a unit domain with arrays of packed spheres has been extracted from Fig. 1a, as shown in Fig. 3a. Here, the packing structure of spheres is selected as SC. The channel height above the spheres is set as $H/R = 32$. A periodic boundary condition with and without a pressure drop Δp is assigned in the x- and y- directions, respectively. For the optimal Stokes–Brinkman coupling, a corresponding effective porous region characterized by K and μ_e is introduced, as shown in Fig. 3b. K is obtained from the fitted Carman–Kozeny model based on the packing structure (SC in this case) and solid volume fraction of the porous media. At the interface, both the continuous and jump stress conditions are considered. The optimal values of μ_e in the continuous stress condition and of the stress jump coefficient in the stress jump condition are obtained from Eqs. (15) and (16), respectively. COMSOL Multiphysics 5.2 is employed to implement all the simulations with the quadratic velocity and linear pressure interpolations. Though not presented here, we have tested the mesh refinement characteristics to ensure an accuracy of over three digits in estimating the slip velocity at the fluid/pore interface. For various solid volume fractions, velocity profiles along a certain line marked as 'l' (see Fig. 3) from the direct simulations and from the Stokes–Brinkman coupling with continuous/jump stress conditions are compared to validate the accuracy of the optimal effective viscosity and stress jump coefficient. Owing to the complex flow behavior

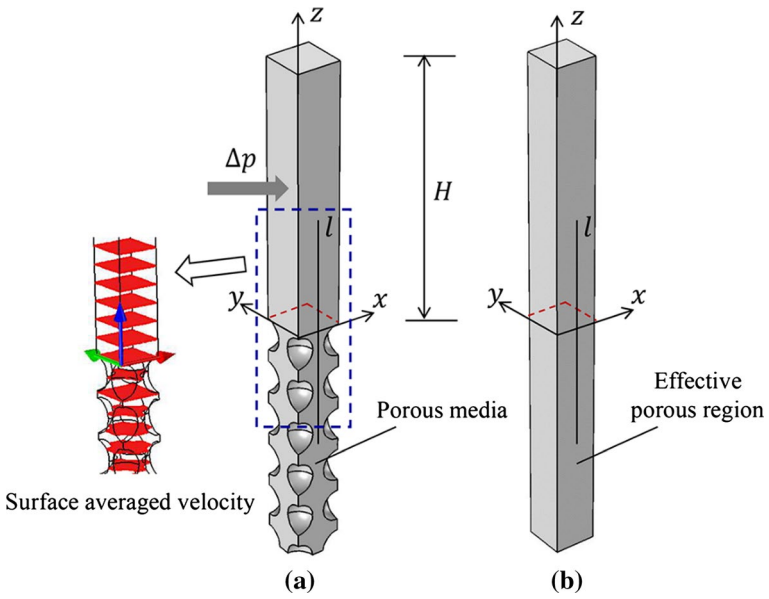

Fig. 3 Computational model for transverse flow over a porous medium composed of packed spheres **a** A model for the direct simulation with the actual complex microarchitecture, **b** the corresponding flow model for Stokes–Brinkman coupling with a fictitious porous region

near the interface, we applied the surface averaged velocity as shown in Fig. 3, to obtain the macro-scale properties, i.e., $u(z) = 1/A_0 \int u dA$. A_0 is the area of cross section for a unit flow region. The results are presented in Fig. 4. Solutions from the continuous stress condition with an identical relative effective viscosity, i.e., $\mu_e = \mu$, are also plotted here for comparison. One can observe that once the optimal parameters $(\mu_e$ and $\beta)$ are selected, the Stokes–Brinkman coupling with both the continuous stress condition and the stress jump condition can accurately reproduce the flow in the fluid region ($z > 0$) and in the porous media ($z < 0$). As expected, with the optimal parameters, solutions from both the continuous stress condition and stress jump condition can accurately predict the slip velocity at the interface ($z = 0$). This is because the optimal expressions of these two parameters are

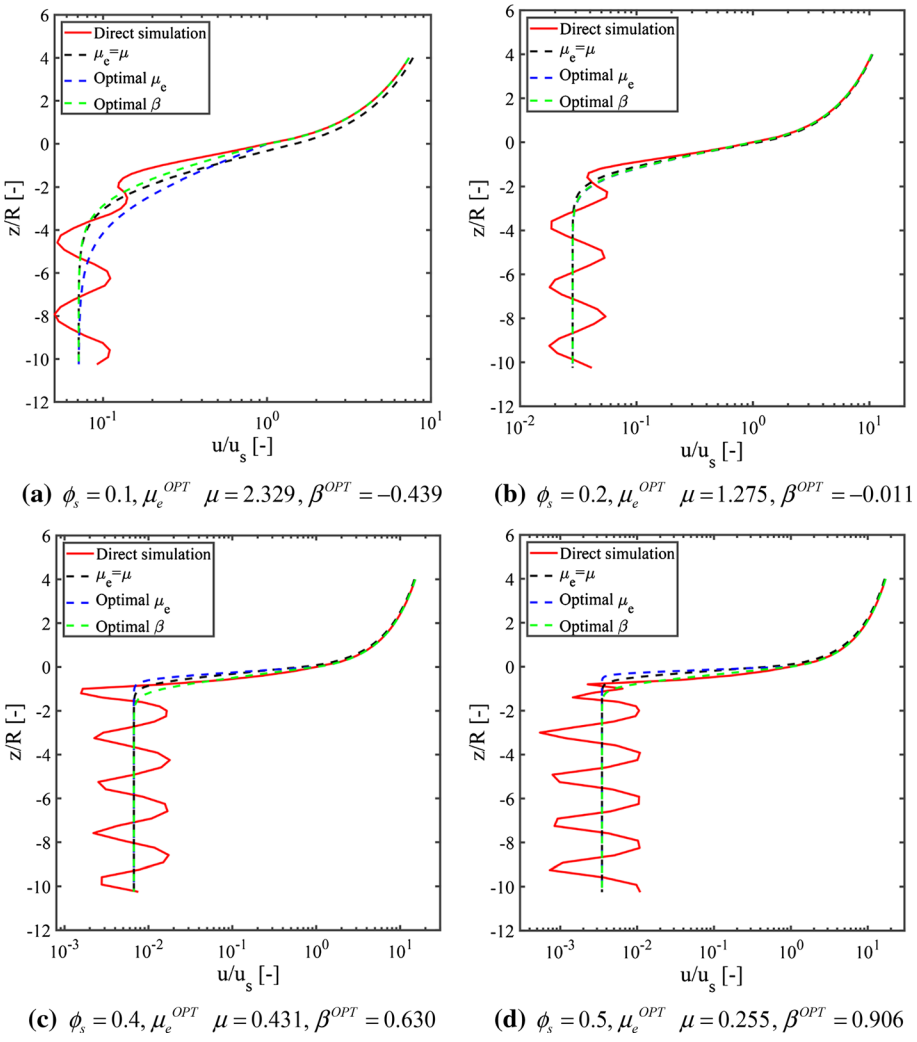

Fig. 4 Velocity profiles along line '*l*' (indicated in Fig. 3) from the direct simulations and the Stokes–Brinkman coupling with optimal effective viscosity and stress jump coefficient for SC packing structure

derived from the Navier-slip condition by matching the slip velocity. However, the continuous stress condition with an identical μ_e $(\mu_e = \mu)$ fails to reproduce the slip velocity. The errors are 50.9% for $\phi_s = 0.1$, 12.9% for $\phi_s = 0.2$, 33.6% for $\phi_s = 0.4$, and 49.1% for $\phi_s = 0.5$. It should be noted that the continuous stress condition with the optimal effective viscosity appears to overestimate the boundary layer thickness for low solid volume fractions (e.g., $\phi_s = 0.1$), whereas it underestimates the boundary layer thickness for high solid volume fractions (e.g., $\phi_s = 0.4$ and $\phi_s = 0.5$). However, for the stress jump condition with the optimal stress jump coefficient, it exhibits best prediction in estimating the boundary layer thickness for various solid volume fractions than the continuous stress condition.

3 Example Flow Problems

After validating the accuracy of the optimal effective viscosity in the continuous stress condition and of the stress jump coefficient in the stress jump condition, in this section, the Stokes–Brinkman coupling with these two parameters is employed to solve two example flow problems: a stick–slip–stick flow and a rectangular channel flow.

3.1 Stick–Slip–Stick Flow

The first example flow problem is a 'stick–slip–stick' flow problem (Fig. 5). A direct simulation (Fig. 5a) is first conducted for a pressure-driven flow over two aligned no-slip solid walls, which are connected by a porous wall composed of eight layers of packed spheres. The packing structure in this case is selected to be SC with solid volume fraction $\phi_s = 0.3$. A periodic boundary condition with and without a pressure drop is assigned in the x- and y- directions, respectively. The depth of the periodic domain is 1 (mm), and the radius of the sphere is 41.5 (μm). The height of the flow channel above the spheres is set as

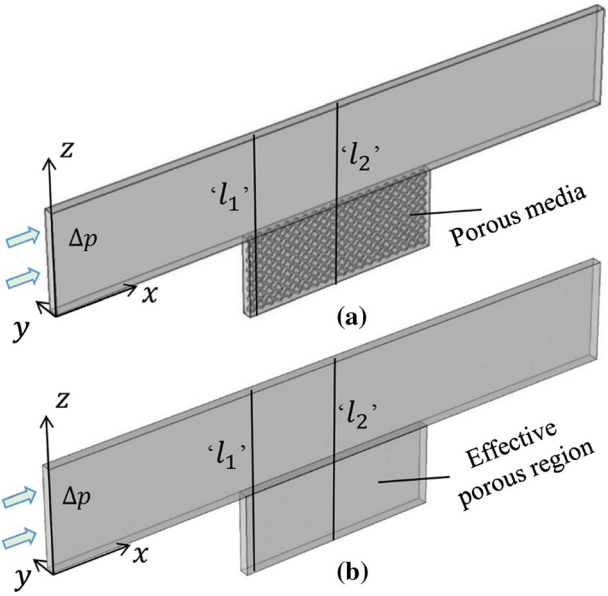

Fig. 5 Schematic description of stick–slip–stick flow **a** computational domain for flow over the actual porous structure composed of packed spheres, **b** computational domain for the Stokes–Brinkman coupling with a fictitious porous region

$H/R = 32$. All the remaining boundaries are subjected to no-slip walls. As reported by Jang et al. (2016), the flow characteristics within a groove, which is analogous to the flow above a porous surface, do not change with respect to the Reynolds number in the laminar regime. Thus, omitting the inertia effect owing to the small scale of the flow problem, a full three-dimensional direct simulation is implemented to solve the Stokes flow problem. In an effective simulation of the Stokes–Brinkman coupling (Fig. 5b), the porous medium is replaced by an effective porous region with K and μ_e. At the fluid/pore interface, both the continuous and jump stress conditions are considered. With the geometry parameters specified above, the optimal relative effective viscosity in the continuous stress condition and the stress jump coefficient in the stress jump condition can be obtained from Eqs. (15) and (16) or Table 1. They are 0.742 and 0.329, respectively. In addition, the stress jump coefficient calculated by the model of Valdés-Parada et al. (2009), which is found to be 1.195 in the present problem, is also considered for comparison. COMSOL 5.2 with the quadratic velocity and the linear pressure interpolations is employed to implement the simulations. Although not presented here, we tested the accuracy of the solution with mesh refinement and assessed the convergence in both the simulations.

Velocity profiles along a centerline located on the bottom wall (see Fig. 5, $z = 0$) from both the direct simulation and the optimal Stokes–Brinkman coupling are shown in Fig. 6. As expected, for the direct simulation, in the upstream region, the velocity from the direct simulation is zero owing to the no-slip property of the solid wall. Then, the velocity increases sharply, and a fluctuation appears between 3.9 and 4.9% of the maximum velocity, caused by the periodic structure of porous media at the interface. The velocity decreases to zero again in the downstream region. For the simulation of the Stokes–Brinkman coupling with the optimal parameters, no evident difference in the velocity profiles can be observed in this case between the continuous stress condition and the stress jump condition. In the porous section, velocity profiles from both the continuous and jump stress conditions are observed to be located in the average position of the fluctuation. The difference of mean velocities from the continuous and jump stress conditions is approximately 1.4% and 1.1%, respectively, of that from the direct simulation. However, in case of the

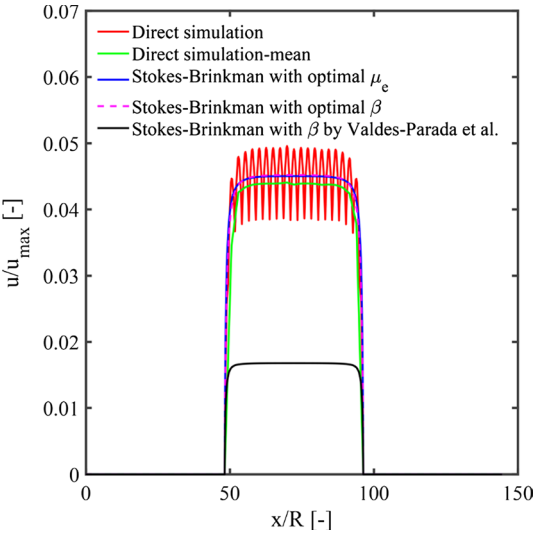

Fig. 6 Velocity profile along centerline located on the bottom surface for the 'stick–slip–stick' flow problem ($z = 0$, Fig. 5) from both direct simulation and simulation of optimal Stokes–Brinkman coupling with both continuous and jump stress conditions. The mean velocity from the direct simulation and the velocity profile in Valdes-Parada et al. (2009) are also presented for comparison

stress jump condition, the model of Valdes-Parada et al. (2009) fails to predict the velocity profile along the porous section, with the relative error being around 61.9%.

Figure 7 shows the velocity profiles along two vertical lines marked as 'l_1' and 'l_2' in Fig. 5, from the direct simulation and those from the optimal Stokes–Brinkman coupling with the continuous and jump stress conditions. No apparent difference in the velocity profiles between the continuous and jump stress conditions is observed, and both of them can accurately reproduce the flow field in the fluid channel ($z > 0$) and within the porous media ($z < 0$). Particularly, for flow in the boundary layer, the velocity profiles in both cases from the Stokes–Brinkman coupling agree well with that from the direct simulation.

3.2 Rectangular Channel Flow

The second example flow problem is a rectangular channel flow bounded by four-layer porous walls attached to the left, right, and top surfaces and a no-slip solid wall at the bottom, as shown in Fig. 8. The local porous architecture is identical to that applied in the stick–slip–stick flow problem. The depth of the periodic domain is 1 [mm], and the radius of the sphere is 41.5 [μm]. The width and height of the channel (excluding the porous layers) are 1.917 [mm] and 1.958 [mm], respectively. For the direct simulation (Fig. 8a), a periodic boundary condition with and without a pressure drop Δp has been assigned in the y- and x-directions, respectively. A symmetry boundary condition is defined on the top surface, whereas the bottom surface yields a no-slip wall. For simulating the Stokes–Brinkman coupling (Fig. 8b), both the continuous and jump stress conditions are employed at the fluid/pore interface, using the optimal effective viscosity and stress jump coefficient, respectively. Although not presented here, the accuracy of the solution with mesh refinement has been assessed in both the simulations.

To assess the performance of the optimal Stokes–Brinkman coupling in this rectangular channel flow problem, velocity profiles along the two lines marked as 'l_3' and 'l_4' (see Fig. 8) from the simulation of the Stokes–Brinkman coupling are compared with those from the direct simulation. As shown in Fig. 9, along line 'l_3,' the velocity increases

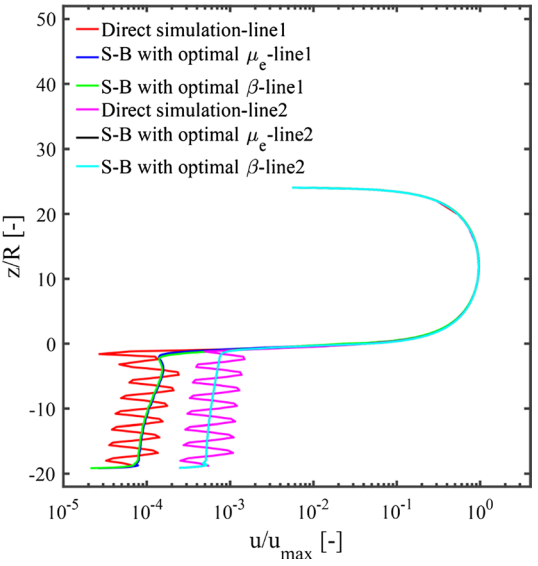

Fig. 7 Velocity profile along two vertical lines (marked as 'l_1' and 'l_2' in Fig. 5) from direct simulation and optimal Stokes–Brinkman coupling with both continuous and jump stress conditions

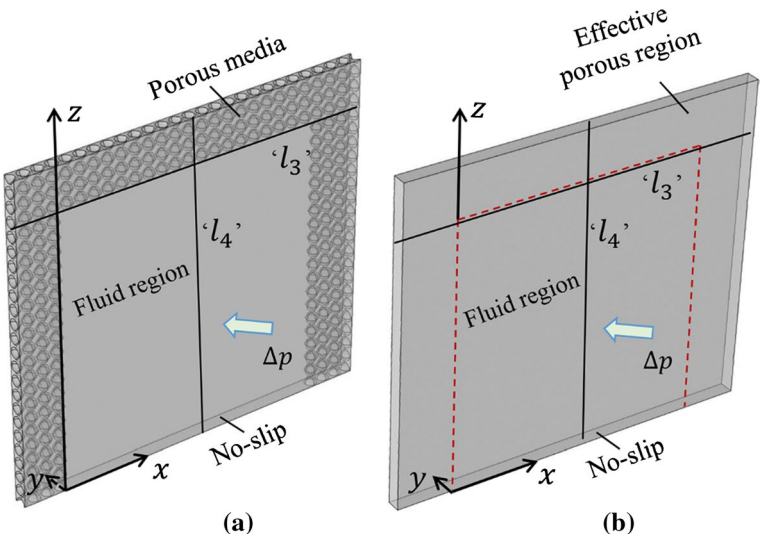

Fig. 8 Schematic description of rectangular channel flow problem **a** direct simulation of channel flow bounded by porous walls adjacent to left, right, and top surfaces, **b** the corresponding effective simulation of Stokes–Brinkman coupling with a fictitious porous region

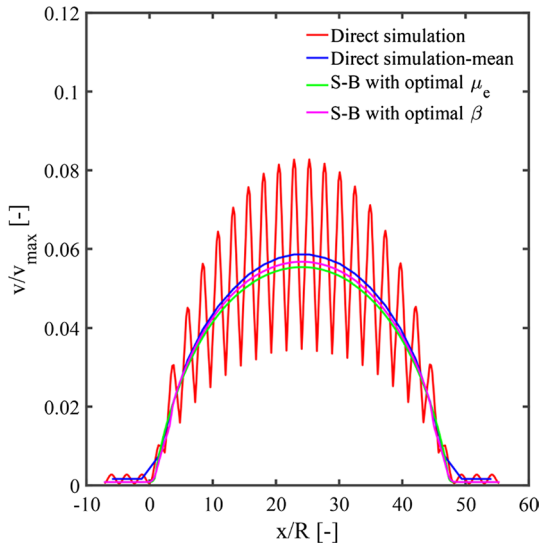

Fig. 9 Velocity profile along the line marked as 'l_3' in Fig. 8, from direct simulation and the corresponding optimal Stokes–Brinkman coupling with both continuous and jump stress conditions

first from the Darcy velocity to the maximum value and then decreases back to the Darcy velocity. In the direct simulation, owing to the periodic porous architecture, a velocity fluctuation appears. In the Stokes–Brinkman coupling, a marginal discrepancy in the velocity profile between the continuous and jump stress conditions is observed. In general, the Stokes–Brinkman coupling with both the continuous and jump stress conditions can accurately reproduce the velocity field in the entire region (pure fluid channel and porous media). Compared to the mean velocity, which is obtained from the direct simulation, the

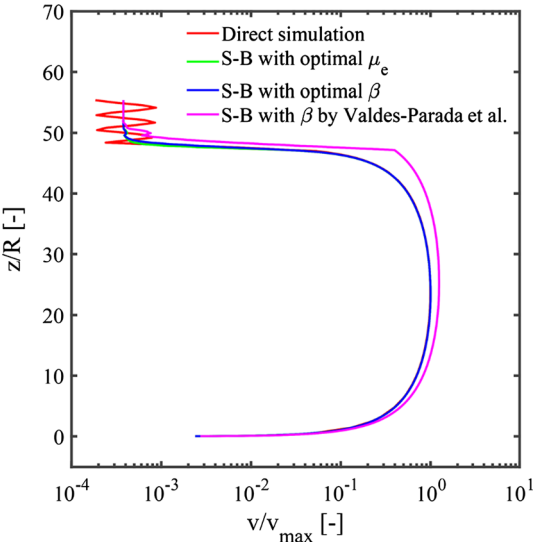

Fig. 10 Velocity profile along the line marked as 'l_4' in Fig. 8, from direct simulation and the corresponding optimal Stokes–Brinkman coupling with both continuous and jump stress conditions. The velocity profile in Valdes-Parada et al. (2009) is also presented for comparison

maximum errors from the continuous stress condition and the stress jump condition are 5.5% and 3.2%, respectively. Figure 10 shows the velocity profile along the line 'l_4' (see Fig. 8) obtained from both the direct simulation and Stokes–Brinkman coupling. No apparent difference in the velocity profiles between the continuous and jump stress conditions is observed. Moreover, there is a good agreement of velocity profiles between the direct simulation and the Stokes–Brinkman coupling in both the fluid region and porous media. In general, once the optimal parameters are chosen, the Stokes–Brinkman coupling with both the stress boundary conditions can accurately predict the local flow field ('l_3') as well as the global flow field ('l_4') in this channel flow problem. In case of the stress jump condition, the model of Valdes-Parada et al. (2009) is also presented for comparison, see Fig. 10. One can observe that the model of Valdes-Parada (2009) overestimates the velocity fields in both the fluid region and porous section.

4 Conclusions

In this work, the Stokes–Brinkman coupling with both the continuous and jump stress conditions have been employed to investigate the flows through a porous medium composed of packed spheres. The slip velocity from the Stokes–Brinkman coupling is matched with that from the Navier-slip condition to obtain the optimal expressions of the effective viscosity and stress jump coefficient. The correlations between the slip length and the effective viscosity as well as stress jump coefficient are determined. The accuracy of these two parameters (the effective viscosity and stress jump coefficient) has been validated by comparing the velocity profiles in both the fluid and porous regions as obtained from the Stokes–Brinkman coupling with those obtained from the direct simulations. The solutions obtained from the stress jump condition are observed to exhibit higher performance in matching the velocity profiles and estimating the boundary layer thickness. The optimal effective viscosity decreases as the solid volume fraction increases, whereas the stress jump coefficient increases with the solid volume fraction. By selecting the optimal

parameters, the Stokes–Brinkman coupling with both the continuous and jump stress conditions are applied to solve two example flow problems, i.e., a stick–slip–stick flow and a channel flow. Both these stress conditions in Stokes–Brinkman coupling exhibit good performances in reproducing the velocity fields in the entire domain.

It is worthwhile to mention that in our approach, the optimal choices of μ_e and β may be considered as properties of the porous architecture. By characterizing the optimal values of these two parameters accurately, the Stokes–Brinkman coupling with a macroscopically characterized porous region can be applied to replace the actual porous media. Thereby, the computing cost is likely to reduce considerably. This work may facilitate the prediction of the voids motion or the particle deposition in porous media, for advanced composites manufacturing.

Acknowledgements The authors acknowledge financial supports from the National Research Foundation of Korea (NRF-2019R1A2C1003974) and from the Korea Agency for Infrastructure Technology Advancement grant funded by Ministry of Land, Infrastructure and Transport (17IFIP-B133614-01, The Industrial Strategic Technology Development Program).

References

Angot, P.: On the well-posed coupling between free fluid and porous viscous flows. Appl. Math. Lett. **24**(6), 803–810 (2011)

Beavers, G.S., Joseph, D.D.: Boundary conditions at a naturally permeable wall. J. Fluid. Mech. **30**(1), 197–207 (1967)

Breugem, W.: The effective viscosity of a channel-type porous medium. Phys. Fluids **19**(10), 103104 (2007)

Brinkman, H.C.: A calculation of the viscous force exerted by a flowing fluid on a dense swarm of particles. Flow Turbul. Combust. **1**(1), 27 (1949)

Chandesris, M., Jamet, D.: Boundary conditions at a fluid–porous interface: an a priori estimation of the stress jump coefficients. Int. J. Heat Mass Transf. **50**(17–18), 3422–3436 (2007)

Chellam, S., Wiesner, M.R.: Slip flow through porous media with permeable boundaries: implications for the dimensional scaling of packed beds. Water Environ. Res. **65**(6), 744–749 (1993)

Esence, T., Bruch, A., Fourmigué, J., Stutz, B.: A versatile one-dimensional numerical model for packed-bed heat storage systems. Renew. Energy **133**, 190–204 (2019)

Gasser, S., Paun, F., Bréchet, Y.: Absorptive properties of rigid porous media: application to face centered cubic sphere packing. J. Acoust. Soc. Am. **117**(4), 2090–2099 (2005)

Goyeau, B., Lhuillier, D., Gobin, D., Velarde, M.G.: Momentum transport at a fluid–porous interface. Int. J. Heat Mass Trans. **46**(21), 4071–4081 (2003)

Hwang, W.R., Advani, S.G.: Numerical simulations of Stokes–Brinkmanequations for permeability prediction of dual scale fibrous porous media. Phys. Fluids **22**(11), 113101 (2010)

Hwang, W.R., Advani, S.G., Walsh, S.: Direct simulations of particle deposition and filtration in dual-scale porous media. Compos. Part A Appl. Sci. Manuf. **42**(10), 1344–1352 (2011)

Jang, H.K., Kim, Y.J., Woo, N.S., Hwang, W.R.: Tensorial navier-slip boundary conditions for patterned surfaces for fluid mixing: numerical simulations and experiments. AIChE J. **62**(12), 4574–4585 (2016)

Llorca, J., Martinez, J.L., Elices, M.: Reinforcement fracture and tensile ductility in sphere-reinforced metal-matrix composites. Fatigue Fract. Eng. Mater. Struct. **20**(5), 689–702 (1997)

Lu, J., Jang, H.K., Lee, S.B., Hwang, W.R.: Characterization on the anisotropic slip for flows over unidirectional fibrous porous media for advanced composites manufacturing. Compos. Part A Appl. Sci. Manuf. **100**, 9–19 (2017)

Lu, X., Xie, P., Ingham, D.B., Ma, L., Pourkashanian, M.: A porous media model for CFD simulations of gas–liquid two-phase flow in rotating packed beds. Chem. Eng. Sci. **189**, 123–134 (2018)

Martys, N., Bentz, D.P., Garboczi, E.J.: Computer simulation study of the effective viscosity in Brinkman's equation. Phys. Fluids **6**(4), 1434–1439 (1994)

Min, J.Y., Kim, S.J.: A novel methodology for thermal analysis of a composite system consisting of a porous medium and an adjacent fluid layer. J. Heat Transf. **127**(6), 648–656 (2005)

Neale, G., Nader, W.: Practical significance of Brinkman's extension of Darcy's law: coupled parallel flows within a channel and a bounding porous medium. Can. J. Chem. Eng. **52**(4), 475–478 (1974)

Ochoa-Tapia, J.A., Whitaker, S.: Momentum transfer at the boundary between a porous medium and a homogeneous fluid—I. Theoretical development. Int. J. Heat Mass Transf. **38**(14), 2635–2646 (1995a)

Ochoa-Tapia, J.A., Whitaker, S.: Momentum transfer at the boundary between a porous medium and a homogeneous fluid—II. Comparison with experiment. Int. J. Heat Mass Transf. **38**(14), 2647–2655 (1995b)

Saleh, S., Thovert, J.F., Adler, P.M.: Flow along porous media by partical image velocimetry. AIChE J. **39**(11), 1765–1776 (1993)

Segurado, J., Llorca, J.: A numerical approximation to the elastic properties of sphere-reinforced composites. J. Mech. Phys. Solids **50**(10), 2107–2121 (2002)

Starov, V.M., Zhdanov, V.G.: Effective viscosity and permeability of porous media. Colloids Surf. Physicochem. Eng. Asp. **192**(1–3), 363–375 (2001)

Takhirov, A.: Stokes–Brinkmanlagrange multiplier/fictitious domain method for flows in pebble bed geometries. SIAM J. Numer. Anal. **51**(5), 2874–2886 (2013)

Tamayol, A., Khosla, A., Gray, B.L., Bahrami, M.: Creeping flow through ordered arrays of micro-cylinders embedded in a rectangular minichannel. Int. J. Heat Mass Transf. **55**(15–16), 3900–3908 (2012)

Tamayol, A., Yeom, J., Akbari, M., Bahrami, M.: Low Reynolds number flows across ordered arrays of micro-cylinders embedded in a rectangular micro/minichannel. Int. J. Heat Mass Transf. **58**(1–2), 420–426 (2013)

Valdes-Parada, F.J., Ochoa-Tapia, J.A., Alvarez-Ramirez, J.: On the effective viscosity for the Darcy–Brinkman equation. Phys. A Stat. Mech. Appl. **385**(1), 69–79 (2007)

Valdés-Parada, F.J., Alvarez-Ramírez, J., Goyeau, B., Ochoa-Tapia, J.A.: Computation of jump coefficients for momentum transfer between a porous medium and a fluid using a closed generalized transfer equation. Transp. Porous Media **78**(3), 439–457 (2009)

Varahasamy, M., Fand, R.M.: Heat transfer by forced convection in pipes packed with porous media whose matrices are composed of spheres. Int. J. Heat Mass Transf. **39**(18), 3931–3947 (1996)

Vignesadler, M., Adler, P.M., Gougat, P.: Transport processes along fractals-The Cantor-Taylor brush. Physicochem. Hydrodyn. **8**(4), 401–422 (1987)